

Validity of the two-band model of bilayer and trilayer graphene in a magnetic field

R. Côté¹ and Manuel Barrette¹

¹Département de physique, Université de Sherbrooke, Sherbrooke, Québec, J1K 2R1, Canada

(Dated: March 15, 2021)

The eigenstates of an electron in the chiral two-dimensional electron gas (C2DEG) formed in an AB-stacked bilayer or an ABC-stacked trilayer graphene is a spinor with 4 or 6 components respectively. These components give the amplitude of the wave function on the 4 or 6 carbon sites in the unit cell of the lattice. In the tight-binding approximation, the eigenenergies are thus found by diagonalizing a 4×4 or a 6×6 matrix. In the continuum approximation where the electron wave vector $k \ll 1/a_0$, with a_0 the lattice constant of the graphene sheets, a common approximation is the two-band model¹ (2BM) where the eigenstates for the bilayer and trilayer systems are described by a two-component spinor that gives the amplitude of the wave function on the two sites with low-energy $|E| \ll \gamma_1$ where γ_1 is the hopping energy between sites that are directly above one another in adjacent layers. The 2BM has been used extensively to study the phase diagram of the C2DEG in a magnetic field as well as its transport and optical properties. In this paper, we use a numerical approach to compute the eigenstates and Landau level energies of the full tight-binding model in the continuum approximation and compare them with the prediction of the 2BM when the magnetic field or an electrical bias between the outermost layers is varied. Our numerical analysis shows that the 2BM is a good approximation for bilayer graphene in a wide range of magnetic field and bias but mostly for Landau level $M = 0$. The applicability of the 2BM in trilayer graphene, even for level $M = 0$, is much more restricted. In this case, the 2BM fails to reproduce some of the level crossings that occur between the sub-levels of $M = 0$.

PACS numbers: 73.21.-b, 73.22.Dj, 73.22.Pr

I. INTRODUCTION

Electrons in AB- or Bernal-stacked bilayer graphene (AB-BLG) and in rhombohedral or ABC-stacked trilayer graphene (ABC-TLG) behave as a chiral two-dimensional electron gas (C2DEG) of Dirac fermions^{1–3} that has transport properties different from those of the conventional 2DEG formed in semiconductor heterostructures. For example, the Landau level spectrum in the simplest (minimal) tight-binding model of a C2DEG is given by $E_M = \text{sgn}(M) \frac{\alpha_0^2}{\gamma_1} \sqrt{|M|(|M|+1)}$ for AB-BLG and $E_M = \text{sgn}(M) \frac{\alpha_0^3}{\gamma_1} \sqrt{(|M|+2)(|M|+1)|M|}$ for ABC-TLG where $M = 0, \pm 1, \pm 2, \dots$ is the Landau level index, γ_1 is the interlayer hopping amplitude, $\alpha_0 = \sqrt{\frac{3}{2} \frac{\gamma_0 a_0}{\ell}}$ (with γ_0 the nearest-neighbor hopping amplitude in each graphene plane), $a_0 = 2.46$ Å is the lattice constant of graphene and $\ell = \sqrt{\frac{\hbar c}{eB}}$ is the magnetic length. This spectrum leads to the anomalous quantum Hall effect with conductivity $\sigma_{xy} = \pm g \frac{e^2}{h} (n + \frac{1}{2})$ where $n = 0, 1, 2, \dots$ with $g = 4$ for AB-BLG and $g = 6$ for ABC-TLG. (For a review of BLG, see Refs. 4–7).

In the above-mentioned graphene systems, each Landau level is fourfold degenerate when counting spin and valley degrees of freedom. Level $M = 0$, however, is an exception. It has an extra *orbital* degeneracy of two for BLG and three for TLG. This, in turn, leads to an eightfold (BLG) or twelvefold (TLG) degeneracy for that level. The extra degeneracy increases the importance of Coulomb interaction in the C2DEG and new broken-symmetry ground states (such as quantum Hall ferromag-

netic states) can occur whose experimental signature is a new plateau in the Hall conductivity.² A very rich phase diagram for the C2DEG in these graphene systems has been predicted at all integer filling factors in $M = 0$ when the magnetic field or the electrical potential difference (or bias Δ_B) is applied between the two outermost layers.^{8–10}

A knowledge of the Landau level spectrum of the AB-BLG and ABC-TLG is necessary to study the phase diagram and transport properties of the C2DEG. The band structures of these two systems are well approximated by a tight-binding Hamiltonian. In the minimal model, i.e. when keeping only the two hopping parameters γ_0 and γ_1 , the dispersion of the four (six) π bands in AB-BLG (ABC-TLG) is as shown in Fig. 1 for a wave vector \mathbf{k} measured from either of the K_+ or K_- valley point. Two low-energy ($|E| \ll \gamma_1$) bands are separated from two or four high-energy bands by a gap $\Delta = \gamma_1$. An electronic state in each band is specified by a four- (BLG) or six- (TLG) component spinor that gives the amplitude of the wave function of each of the four or six sites in the unit cell of the lattice.

When the Fermi level is close to the degeneracy point of the two middle bands in Fig. 1 and only the low-energy properties of the excited states of the C2DEG are of interest, the complexity of these two graphene systems can be substantially reduced by using an effective two-band model (2BM) for BLG^{1,7} and TLG.^{11,12} This model makes use of the fact that, for an electronic state in one of the two low-energy bands, the amplitude of the different components in the four- or six-component spinor is important only on two low-energy sites. The high-energy sites can thus be integrated out. The Hamiltonian is then

reduced to a 2×2 matrix and the eigenstates are given by a two-component spinor. For completeness, the 2BM is reviewed in Appendix A.

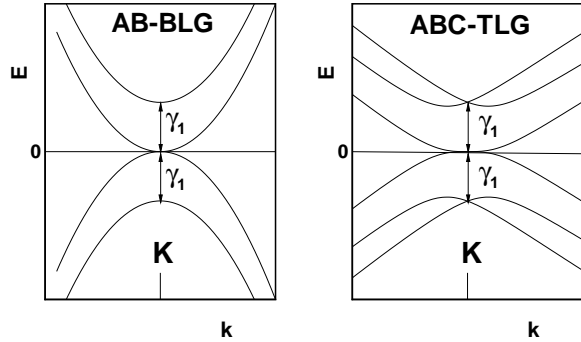


FIG. 1: Schematic drawing of the band structure of AB-stacked bilayer graphene (left) and ABC-stacked trilayer graphene (right) in the minimal model for wave vector \mathbf{k} near the valley point K .

The 2BM has been used extensively in the literature to study the phase diagram of the C2DEG as well as its transport and optical properties.^{8–10,13,14} The phase diagram, up to now, has been mostly studied as a function of magnetic field and bias Δ_B , and at integer filling of the eight or twelve sub-Landau levels in $M = 0$. To appreciate these studies or add corrections such as screening where Landau levels $|M| > 0$ are important, or to study the phase diagram in higher Landau levels, one must know the limits of validity of the 2BM. In the perturbation theory outlined in Appendix A, the 2BM for BLG is estimated to be valid for low-energy excitations $|E| \ll \gamma_1$, and for magnetic field such that $\gamma_1 v_3/v_0^2 < \hbar/\ell < \gamma_1/2v_0$ where $v_i = \frac{\sqrt{3} a_0}{2\hbar} |\gamma_i|$ and γ_3 is the so-called warping term. A similar condition also applies in TLG.

In this work, we use a numerical approach to obtain a more precise evaluation of the range of validity of the 2BM. A numerical computation of the Landau level energies and eigenstates allows the inclusion of all important hopping terms in the tight-binding model and thus give a more realistic description of the levels that goes beyond that of the minimal model^{15–17} when values of the hopping parameters typical of those found in the literature^{12,18} are used. We compare the Landau level energies and eigenstates in the full tight-binding model (in the continuum approximation) with the predictions of the 2BM in a wide range of magnetic field and bias. In our study, we pay particular attention to the eight (BLG) or twelve (TLG) states in $M = 0$ since it is for these levels that the 2BM is best suited.

This paper is organized in the following way. In Sec. II, we introduce the AB-BLG and ABC-TLG systems as well as the tight-binding models that give the Landau level spectrum of the full tight-binding model (4BM or 6BM) and of the effective 2BM. In Sec. III, we discuss

the effect of the different hopping parameters γ_i on the Landau level spectrum, we compare the full and effective models for different values of the warping terms γ_2, γ_3 , bias and magnetic field and discuss the range of validity of the effective model by comparing the eigenenergies and eigenstates in the two models. We conclude in Sec. IV. In Appendix A, we review the derivation of the 2BM.

II. AB-BILAYER AND ABC-TRILAYER GRAPHENE

The crystal structures of the AB-BLG and ABC-TLG (hereafter abbreviated as BLG and TLG) are given in Fig. 2(a),(b) and their tight-binding parameters are defined in Fig. 2(b),(c). (Note that a different labelling is used for equivalent sites in the two structures.) The crystal structure in each graphene layer is a honeycomb lattice that can be described as a triangular Bravais lattice with a basis of two carbon atoms A_n and B_n where n is the layer index. The triangular lattice constant $a_0 = 2.46 \text{ \AA} = \sqrt{3}c$, where $c = 1.42 \text{ \AA}$ is the separation between two adjacent carbon atoms. The unit cell of the BLG (TLG) structure has four (six) carbon atoms. The distance between two adjacent graphene layers is $d \approx 3.4 \text{ \AA}$. The Brillouin zone of the reciprocal lattice is hexagonal and has two nonequivalent valley points $\mathbf{K}_\xi = \left(\frac{2\pi}{a_0} \right) (\xi \frac{2}{3}, 0)$ where $\xi = \pm$ is the valley index.

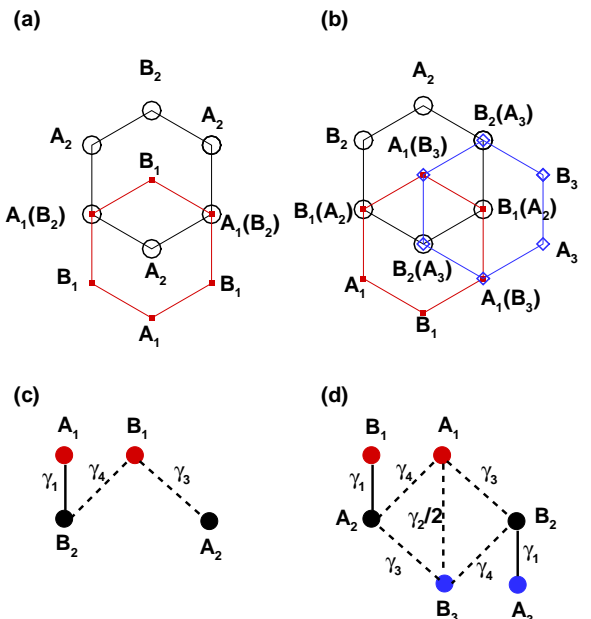


FIG. 2: (Color online) Crystal structure of the (a) Bernal-stacked bilayer graphene and (b) ABC-stacked trilayer graphene. Definition of the hopping parameters for the: (c) bilayer and (d) trilayer systems.

The band structure of BLG or TLG is obtained with a tight-binding Hamiltonian^{1,11,12,19}. The hopping parameters common to both structures are: γ_0 the nearest-neighbor (NN) hopping in each layer, γ_1 the interlayer hopping between carbon atoms that are immediately above one another, γ_3 the interlayer NN hopping term between carbon atoms of different sublattices, and γ_4 the interlayer next NN hopping term between carbon atoms in the same sublattice. In the trilayer, the extra hopping term γ_2 connects the two low-energy sites A_1 and B_3 in Fig. 2.

In the continuum approximation, the tight-binding Hamiltonian is expanded to linear order in the wave vector $\mathbf{p}_\pm = \mathbf{k} - \mathbf{K}_\pm$. The effect of a magnetic field $\mathbf{B} = B\hat{\mathbf{z}}$ perpendicular to the graphene layers is then taken into account by making the Peierls substitution $\mathbf{p} \rightarrow \mathbf{P} = \mathbf{p} + e\mathbf{A}/\hbar c$ (with $e > 0$ for an electron), where \mathbf{A} is the vector potential of the magnetic field.

A. AB bilayer graphene

In a magnetic field, the tight-binding Hamiltonian in the basis $\{A_1, B_1, A_2, B_2\}$ for valley K_- and $\{B_2, A_2, B_1, A_1\}$ for valley K_+ is given by

$$H_\xi = \begin{pmatrix} \delta_0 - \xi \frac{\Delta_B}{2} & \xi \alpha_0 a & \xi \alpha_4 a^\dagger & -\gamma_1 \\ \xi \alpha_0 a^\dagger & -\xi \frac{\Delta_B}{2} & \xi \alpha_3 a & \xi \alpha_4 a^\dagger \\ \xi \alpha_4 a & \xi \alpha_3 a^\dagger & \xi \frac{\Delta_B}{2} & \xi \alpha_0 a \\ -\gamma_1 & \xi \alpha_4 a & \xi \alpha_0 a^\dagger & \delta_0 + \xi \frac{\Delta_B}{2} \end{pmatrix}, \quad (1)$$

where

$$\alpha_i = \sqrt{\frac{3}{2}} \frac{a_0}{\ell} \gamma_i, \quad (2)$$

and δ_0 represents the difference in the crystal field between sites A_1, B_2 and A_2, B_1 . The energy Δ_B is the potential difference (or bias) between the two outermost layers due to an external electric field perpendicular to the layers.

The Hamiltonian $H_\xi^{(0)}$ obtained from H_ξ by setting $\alpha_3 = 0$ has eigenvalues $E_{N,j}^{(0)}$ and eigenspinors of the form

$$\Psi_{N,j,X}^{(0)}(\mathbf{r}) = \begin{pmatrix} c_{N,j,1} h_{N-1,X}(\mathbf{r}) \\ c_{N,j,2} h_{N,X}(\mathbf{r}) \\ c_{N,j,3} h_{N-2,X}(\mathbf{r}) \\ c_{N,j,4} h_{N-1,X}(\mathbf{r}) \end{pmatrix}, \quad (3)$$

where $N \geq 0$. In the Landau gauge $\mathbf{A} = (0, Bx, 0)$, the functions $h_{n,X}(\mathbf{r})$ are given by

$$h_{n,X}(\mathbf{r}) = \frac{1}{\sqrt{L_y}} e^{-iXy/\ell^2} \varphi_n(x - X), \quad (4)$$

where L_y is the length of the 2DEG in the y direction, X the guiding-center index, $\ell = \sqrt{\hbar c/eB}$ the magnetic length and $\varphi_n(x)$ are the wave functions of

the one-dimensional harmonic oscillator with quantum number $n = 0, 1, 2, \dots$. The ladder operators are defined such that $a\varphi_n(x) = -i\sqrt{n}\varphi_{n-1}(x)$ and $a^\dagger\varphi_n(x) = i\sqrt{n+1}\varphi_{n+1}(x)$.

The eigenvalues and coefficients $c_{N,j,k}$ for the eigenvectors are found by diagonalizing the matrix

$$F_1 = \begin{pmatrix} \delta_0 - \xi \frac{\Delta_B}{2} & -\xi \alpha_0 g_N & \xi \alpha_4 i g_{N-1} & -\gamma_1 \\ i \xi \alpha_0 g_N & -\xi \frac{\Delta_B}{2} & 0 & \xi \alpha_4 i g_N \\ -i \xi \alpha_4 g_{N-1} & 0 & \xi \frac{\Delta_B}{2} & -\xi i \alpha_0 g_{N-1} \\ -\gamma_1 & -\xi i \alpha_4 g_N & \xi i \alpha_0 g_{N-1} & \delta_0 + \xi \frac{\Delta_B}{2} \end{pmatrix}. \quad (5)$$

In $\Psi_{N,j,X}^{(0)}(\mathbf{r})$ and in the above equation (and similar ones below), we define $h_{N,X}(\mathbf{r}) = 0$ if $N < 0$ and

$$g_N = \Theta(N) \sqrt{N}, \quad (6)$$

where $\Theta(N)$ is the step function. For example, with $N = 0$, there can be only one eigenspinor ($j = 1$) which is given by (we drop hereafter the \mathbf{r} -dependency to simplify the notation) $\Psi_{0,1,X}^{(0)} = (0, h_{0,X}, 0, 0)$ and its energy is precisely $E_{0,1}^{(0)} = -\xi \frac{\Delta_B}{2}$. For $N = 1$, there are three eigenstates ($j = 1, 2, 3$) and four for $N > 1$ (i.e. $j = 1, 2, \dots, 4$). The energies $E_{N,j}^{(0)}$ and coefficients $c_{N,j,k}$ ($k = 1, 2, 3, 4$) are independent of the guiding-center index X so that the Landau levels have the usual degeneracy $N_\varphi = S/2\pi\ell^2$ where S is the 2DEG area. (These energies and coefficients also depend on the valley index ξ but we do not indicate this in order to simplify the notation.) In the basis $\{\Psi_{N,j,X}^{(0)}\}$ of the eigenspinors of $H_\xi^{(0)}$, the matrix elements

$$\langle \Psi_{N,j,X}^{(0)} | H_\xi^{(0)} | \Psi_{M,k,X'}^{(0)} \rangle = \delta_{X,X'} \delta_{N,M} \delta_{j,k} E_{N,j}^{(0)}. \quad (7)$$

The effect of the warping term α_3 is obtained by diagonalizing the full matrix $H_\xi = H_\xi^{(0)} + W_\xi$ where W_ξ contains only the α_3 terms and has the matrix elements

$$\begin{aligned} & \langle \Psi_{N,j,X}^{(0)} | W_\xi | \Psi_{M,k,X'}^{(0)} \rangle \\ &= -i \xi \alpha_3 \sqrt{M-2} c_{N,j,2}^* c_{M,k,3} \delta_{N,M-3} \delta_{X,X'} \\ &+ i \xi \alpha_3 \sqrt{M+1} c_{N,j,3}^* c_{M,k,2} \delta_{N,M+3} \delta_{X,X'} \end{aligned} \quad (8)$$

This perturbation couples the eigenspinors $\Psi_{N,j,X}^{(0)}$ with the same X and, in view of Eq. (7), the matrix to diagonalize is the same for all X' s. We thus drop the X index hereafter. If the highest Landau level kept in the calculation is N_{\max} , then the matrix for H_ξ to diagonalize has order $4N_{\max}$.

The two-band model for bilayer graphene^{1,7} can be obtained in a number of ways. We describe one such way in Appendix A. In the basis (B_1, A_2) for K_- and (A_2, B_1) for K_+ , the effective two-band Hamiltonian is

$$\tilde{H}_\xi = \begin{pmatrix} -\xi \frac{\Delta_B}{2} + \zeta_+ a^\dagger a & \frac{\alpha_0^2}{\gamma_1} (a^\dagger)^2 \\ \frac{\alpha_0^2}{\gamma_1} a^2 & \xi \frac{\Delta_B}{2} + \zeta_- a a^\dagger \end{pmatrix}, \quad (9)$$

where

$$\beta = \frac{\alpha_0}{\gamma_1}, \quad (10)$$

$$\zeta = 2\beta\alpha_4 + \beta^2\delta_0, \quad (11)$$

$$\zeta_{\pm} = \zeta \pm \xi\beta^2\Delta_B, \quad (12)$$

The 2BM, as we define it here, does not include the warping term γ_3 .

The eigenspinors of the 2BM are of the form

$$\tilde{\Psi}_{N,j} = \begin{pmatrix} c_{N,j,1}h_N \\ c_{N,j,2}h_{N-2} \end{pmatrix}. \quad (13)$$

The $N = 0$ eigenvector (with $j = 1$) is $\tilde{\Psi}_{0,1} = (h_0, 0)$ and has energy

$$\tilde{E}_{0,1}^{(0)} = -\xi \frac{\Delta_B}{2}. \quad (14)$$

For $N = 1$, the eigenvector (with $j = 1$) is $\tilde{\Psi}_{1,1} = (h_1, 0)$ with energy

$$\tilde{E}_{1,1}^{(0)} = -\xi \frac{\Delta_B}{2} + \zeta_+. \quad (15)$$

The Landau levels are obtained by diagonalizing the matrix

$$F_2 = \begin{pmatrix} -\xi \frac{\Delta_B}{2} + \zeta_+ g_N^2 & -\frac{\alpha_0^2}{\gamma_1} g_N g_{N-1} \\ -\frac{\alpha_0^2}{\gamma_1} g_N g_{N-1} & \xi \frac{\Delta_B}{2} + \zeta_- g_{N-1}^2 \end{pmatrix}. \quad (16)$$

For $N > 1$, the index $j = 1, 2$.

In the minimal model ($\gamma_0, \gamma_1 \neq 0$ only), the Landau level spectrum is given by $E_M = \text{sgn}(M) \frac{\alpha_0^2}{\gamma_1} \sqrt{|M|(|M|+1)}$. The $N = 0$ and $N = 1$ states are degenerate and are part of the Landau level $M = 0$. Below we refer to these states as the states $n = 0$ and $n = 1$ of $M = 0$ where n is the *orbital* index in the eigenspinor $(h_n, 0)$. The index $N \geq 0$ that we use to classify the Landau levels in our numerical analysis is different from the Landau level M . For $N \geq 2$ in Eq. (16), the relation is $M = \pm(N-1)$.

B. ABC-stacked trilayer graphene

We repeat the above procedure to get the Landau levels of the ABC-TLG. The tight-binding Hamiltonian in the basis $(A_1, B_3, B_1, A_2, B_2, A_3)$ for K_+ and $(B_3, A_1, A_3, B_2, A_2, B_1)$ for K_- is

$$H_{\xi} = \begin{pmatrix} \xi \frac{\Delta_B}{2} + \delta_0 & \frac{\gamma_2}{2} & \xi\alpha_0 a & \xi\alpha_4 a & \xi\alpha_3 a^\dagger & 0 \\ \frac{\gamma_2}{2} & -\xi \frac{\Delta_B}{2} + \delta_0 & 0 & \xi\alpha_3 a & \xi\alpha_4 a^\dagger & \xi\alpha_0 a^\dagger \\ \xi\alpha_0 a^\dagger & 0 & \xi \frac{\Delta_B}{2} & \gamma_1 & \xi\alpha_4 a & 0 \\ \xi\alpha_4 a^\dagger & \xi\alpha_3 a^\dagger & \gamma_1 & 0 & \xi\alpha_0 a & \xi\alpha_4 a \\ \xi\alpha_3 a & \xi\alpha_4 a & \xi\alpha_4 a^\dagger & \xi\alpha_0 a^\dagger & 0 & \gamma_1 \\ 0 & \xi\alpha_0 a & 0 & \xi\alpha_4 a^\dagger & \gamma_1 & -\xi \frac{\Delta_B}{2} \end{pmatrix}, \quad (17)$$

where the energy δ_0 represents the difference in the crystal field between sites A_1, B_3 and sites A_2, A_3, B_1, B_2 . (In Eq. (17), it is assumed that the middle layer is at zero potential and that Δ_B is the potential difference between the two outermost layers.)

We define $H_{\xi}^{(0)}$ as the Hamiltonian with γ_3 and γ_2 set to zero. Its eigenspinors are of the form

$$\Psi_{N,j}^{(0)} = \begin{pmatrix} c_{N,j,1}h_{N-3} \\ c_{N,j,2}h_N \\ c_{N,j,3}h_{N-2} \\ c_{N,j,4}h_{N-2} \\ c_{N,j,5}h_{N-1} \\ c_{N,j,6}h_{N-1} \end{pmatrix}. \quad (18)$$

There is only one solution for $N = 0$ (with the energy $E_{0,1}^{(0)} = -\xi \frac{\Delta_B}{2} + \delta_0$ and $j = 1$), three solutions for $N = 1$ ($j = 1, 2, 3$), five solutions for $N = 2$ (i.e. $j = 1, 2, \dots, 5$) and six for $N > 2$ (i.e. $j = 1, 2, \dots, 6$). The matrix to diagonalize is

$$F_3 = \begin{pmatrix} \xi \frac{\Delta_B}{2} + \delta_0 & 0 & -i\xi\alpha_0 g_{N-2} & -i\xi\alpha_4 g_{N-2} & 0 & 0 \\ 0 & -\xi \frac{\Delta_B}{2} + \delta_0 & 0 & 0 & i\xi\alpha_4 g_N & i\xi\alpha_0 g_N \\ i\xi\alpha_0 g_{N-2} & 0 & \xi \frac{\Delta_B}{2} & \gamma_1 & -i\xi\alpha_4 g_{N-1} & 0 \\ i\xi\alpha_4 g_{N-2} & 0 & \gamma_1 & 0 & -i\xi\alpha_0 g_{N-1} & -i\xi\alpha_4 g_{N-1} \\ 0 & -i\xi\alpha_4 g_N & i\xi\alpha_4 g_{N-1} & i\xi\alpha_0 g_{N-1} & 0 & \gamma_1 \\ 0 & -i\xi\alpha_0 g_N & 0 & i\xi\alpha_4 g_{N-1} & \gamma_1 & -\xi \frac{\Delta_B}{2} \end{pmatrix}. \quad (19)$$

The Landau levels are obtained by diagonalizing the full matrix $H_{\xi} = H_{\xi}^{(0)} + W_{\xi}$ where W_{ξ} contains only the

elements of H_{ξ} with γ_2 and α_3 . The matrix elements of W_{ξ} in the basis $\{\Psi_{N,j}^{(0)}\}$ of the eigenvectors of $H_{\xi}^{(0)}$ are

given by

$$\begin{aligned} & \left\langle \Psi_{N,j}^{(0)} | W_\xi | \Psi_{M,k}^{(0)} \right\rangle \quad (20) \\ &= \frac{\gamma_2}{2} (\delta_{N-3,M} c_{N,j,1}^* c_{M,k,2} + \delta_{N+3,M} c_{N,j,2}^* c_{M,k,1}) \\ & \quad - \delta_{N+3,M} i \xi \alpha_3 (c_{N,j,2}^* c_{M,k,4} g_{M-2} + c_{N,j,5}^* c_{M,k,1} g_{M-3}) \\ & \quad + \delta_{N-3,M} i \xi \alpha_3 (c_{N,j,4}^* c_{M,k,2} g_{M+1} + c_{N,j,1}^* c_{M,k,5} g_M). \end{aligned}$$

If the highest Landau level kept in the calculation is N_{\max} , the matrix to diagonalize has order $6(N_{\max} - 2) + 9$.

For the two-band model, the basis is (A_1, B_3) for H_{K_+} and (B_3, A_1) for H_{K_-} and the Hamiltonian is given by

$$\tilde{H}_\xi = \begin{pmatrix} \delta_0 + \xi \frac{\Delta_B}{2} - \tilde{\zeta}_+ a a^\dagger & \xi \frac{\alpha_0^3}{\gamma_1^2} a^3 \\ \xi \frac{\alpha_0^3}{\gamma_1^2} (a^\dagger)^3 & \delta_0 - \xi \frac{\Delta_B}{2} - \tilde{\zeta}_- a^\dagger a \end{pmatrix}. \quad (21)$$

It does not include the γ_2 and γ_3 couplings. In this equation,

$$\tilde{\zeta}_\pm = \zeta \pm \frac{1}{2} \xi \beta^2 \Delta_B. \quad (22)$$

The eigenvectors of \tilde{H}_ξ have the form

$$\tilde{\Psi}_{N,j} = \begin{pmatrix} c_{N,j,1} h_{N-3} \\ c_{N,j,2} h_N \end{pmatrix}. \quad (23)$$

There is one solution only (i.e. $j = 1$) for $N = 0, 1, 2$ which are $\tilde{\Psi}_{0,1} = (0, h_0)$, $\tilde{\Psi}_{1,1} = (0, h_1)$, $\tilde{\Psi}_{2,1} = (0, h_2)$ with energy

$$\tilde{E}_{0,1} = \delta_0 - \xi \frac{\Delta_B}{2}, \quad (24)$$

$$\begin{aligned} \tilde{E}_{1,1} &= (1 - \beta^2) \delta_0 \\ & - \xi (1 - \beta^2) \frac{\Delta_B}{2} - 2\beta\alpha_4, \end{aligned} \quad (25)$$

and

$$\begin{aligned} \tilde{E}_{2,1} &= (1 - 2\beta^2) \delta_0 \\ & - \xi (1 - 2\beta^2) \frac{\Delta_B}{2} - 4\beta\alpha_4. \end{aligned} \quad (26)$$

For $N > 2$, there are two solutions and the index $j = 1, 2$.

As in BLG, these three solutions are degenerate in the minimal model and they belong to Landau level $M = 0$. Below, we refer to them as the orbital states $n = 0, 1, 2$ of $M = 0$. The Landau level quantization in the minimal model is $E_M = \text{sgn}(M) \frac{\alpha_0^3}{\gamma_1^2} \sqrt{(|M|+2)(|M|+1)|M|}$ while, for \tilde{H}_ξ , the Landau level spectrum is obtained by diagonalizing the matrix

$$F_4 = \begin{pmatrix} \delta_0 + \xi \frac{\Delta_B}{2} - \tilde{\zeta}_+ g_{N-2}^2 & i \xi \frac{\alpha_0^3}{\gamma_1^2} g_N g_{N-1} g_{N-2} \\ -i \xi \frac{\alpha_0^3}{\gamma_1^2} g_N g_{N-1} g_{N-2} & \delta_0 - \xi \frac{\Delta_B}{2} - \tilde{\zeta}_- g_N^2 \end{pmatrix}. \quad (27)$$

With $N \geq 3$ in F_4 , we obtain the energy of the Landau levels $M = \pm(N-2)$.

III. NUMERICAL RESULTS

Each of the four or six bands in the band structure shown in Fig. 1 leads to a set of Landau levels. Since we are interested in comparing the full four-band (4BM) or six-band (6BM) models with the 2BM, we need to consider only the Landau levels originating from the two low-energy bands. In addition, the Landau level spectrum has the symmetry $E_{N,j}(\xi, \Delta_B) = E_{N,j}(-\xi, -\Delta_B)$ and so we can further restrict our analysis to the spectrum in one valley. We choose the valley K_+ . For the numerical calculations, we use the parameters: $\gamma_0 = 3.16$ eV, $\gamma_1 = 0.502$ eV, $\gamma_2 = -0.0171$ eV, $\gamma_3 = -0.377$ eV, $\gamma_4 = -0.099$ eV, $\delta_0 = -0.0014$ eV for TLG¹² and $\gamma_0 = 3.12$ eV, $\gamma_1 = 0.39$ eV, $\gamma_3 = 0.29$ eV, $\gamma_4 = 0.12$ eV, $\delta_0 = 0.0156$ eV for BLG^{18,20}. These parameters are not all precisely known and can be affected by correlation effects and substrate.²¹ However, small changes from these values should not affect significantly our conclusions concerning the validity of the 2BM.

A. Analytical criteria for the validity of the two-band model

For the 2BM to be a valid approximation, the energy $|E|$ of the Landau levels must be much smaller than the inter-layer hopping energy γ_1 i.e. smaller than the energy of the higher-energy bands. In the minimal model $E \sim \alpha_0^2/\gamma_1$ for BLG and $E \sim \alpha_0^3/\gamma_1^2$ for TLG. If we require that $E < \gamma_1/4$, then the condition of validity of the 2BM¹ is $\hbar/\ell < \gamma_1/2v_0$ (BLG) and $\hbar/\ell < \gamma_1/2^{4/3}v_0$ (TLG), where $v_i = \frac{\sqrt{3}}{2} \frac{\alpha_0}{\hbar} |\gamma_i|$. For our choice of parameters, this condition implies that $B \lesssim 56$ T for BLG and TLG.

The warping terms γ_2, γ_3 can also be included in the 2BM. For BLG, this means adding to the Hamiltonian in Eq. (9) the term

$$\tilde{H}_{w,\xi} = \xi \alpha_3 \begin{pmatrix} 0 & a \\ a^\dagger & 0 \end{pmatrix} \quad (28)$$

and computing the eigenvalues numerically. For TLG, the warping term γ_3 contributes¹¹ a term of order $2\alpha_0\alpha_3/\gamma_1$. If we require the warping term energy to be smaller than the typical Landau level energy, then we need $\hbar/\ell > \gamma_1 v_3/v_0^2$ for BLG and $\hbar/\ell > 2\gamma_1 v_3/v_0^2$ for TLG. With our choice of parameters, this implies $B \gtrsim 2$ T for BLG and $B \gtrsim 21$ T for TLG. In TLG, we arrive at approximately the same magnetic field if we require that $|\gamma_2|/2 < \alpha_0^3/\gamma_1^2$, where $|\gamma_2|/2$ is the typical energy contribution for the hopping term γ_2 .

B. Effect of the hopping terms γ_2, γ_3

We start our analysis by looking at the effect of the hopping terms γ_2 and γ_3 that couple the eigenspinors

$\Psi_{N,j}^{(0)}$ together. For an AB-BLG, the effect of the warping term γ_3 is discussed in Ref. 1 but within the 2BM. Fig. 3 of that paper shows how the γ_3 term couples the Landau levels in the 2BM when $\gamma_4, \delta_0 = 0$. For small $\alpha = \gamma_3/\gamma_0$, the Landau level spectrum is almost independent of γ_3 while, at larger value of α , groups of four consecutive levels become degenerate, each group being separated from the next by two nondegenerate Landau levels. In BLG, the value of $\gamma_3/\gamma_0 \approx 0.09$ is such that γ_3 has very little effect on the spectrum if the magnetic field is large enough i.e. for $B \gtrsim 1$ T. This is in good agreement with the analytical result given previously.

Figure 3 of our paper shows our numerical results for the effect of γ_3 on the Landau level spectrum but calculated in the 4BM. We reach the same conclusion as in Ref. 1 i.e. the warping term affects the spectrum only at very small magnetic field. For $B \gtrsim 1$ T, the effect of γ_3 is already very small. The dispersion of the levels with γ_3/γ_0 , however, is qualitatively different than that of the 2BM. In the 4BM, groups of three instead of four consecutive levels become degenerate. We can reproduce this behavior with the 2BM if we include γ_3 and γ_4 in the two-band Hamiltonian i.e. if we add to Eq. (9) the warping term of Eq. (28) and solve using the procedure described in Sec. II. The dispersion of the resulting levels is shown by the blue squares in Fig. 3. Note that, in this figure, the magnetic field is small and so the 4BM and 2BM (with warping) are in good agreement.

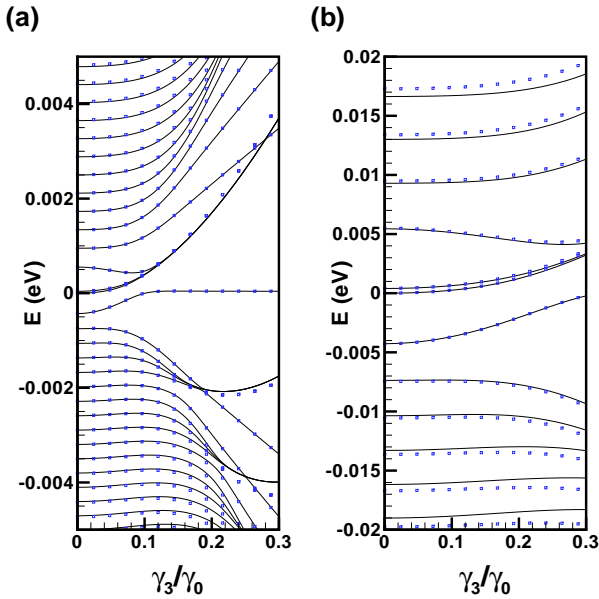


FIG. 3: Landau level spectrum as a function of the ratio γ_3/γ_0 at zero bias in the four-band (lines) and two-band (blue squares) model of BLG for (a) $B = 0.1$ T and (b) $B = 1.0$ T. The two-band model considered in this figure includes the warping term γ_3 .

In the 6BM of TLG, the γ_2 term leads to Landau levels that are degenerate by groups of three at small magnetic

field (see also Fig. 9 (d) below). We thus set this term to zero in order to study the effect of the warping term γ_3 . At field $B = 0.1$ T, Fig. 4 (a) shows that the warping term leads to an important modification of the Landau level spectrum for $|\gamma_3/\gamma_0| = 0.12$ corresponding to the estimated value of the ratio of γ_3 and γ_0 in TLG. At the larger magnetic field $B = 10$ T, Fig. 4 (b) shows that the effect of γ_3 is still noticeable. It becomes negligible at a magnetic field $B \approx 20$ T (this can also be seen in Fig. 5 (d) below).

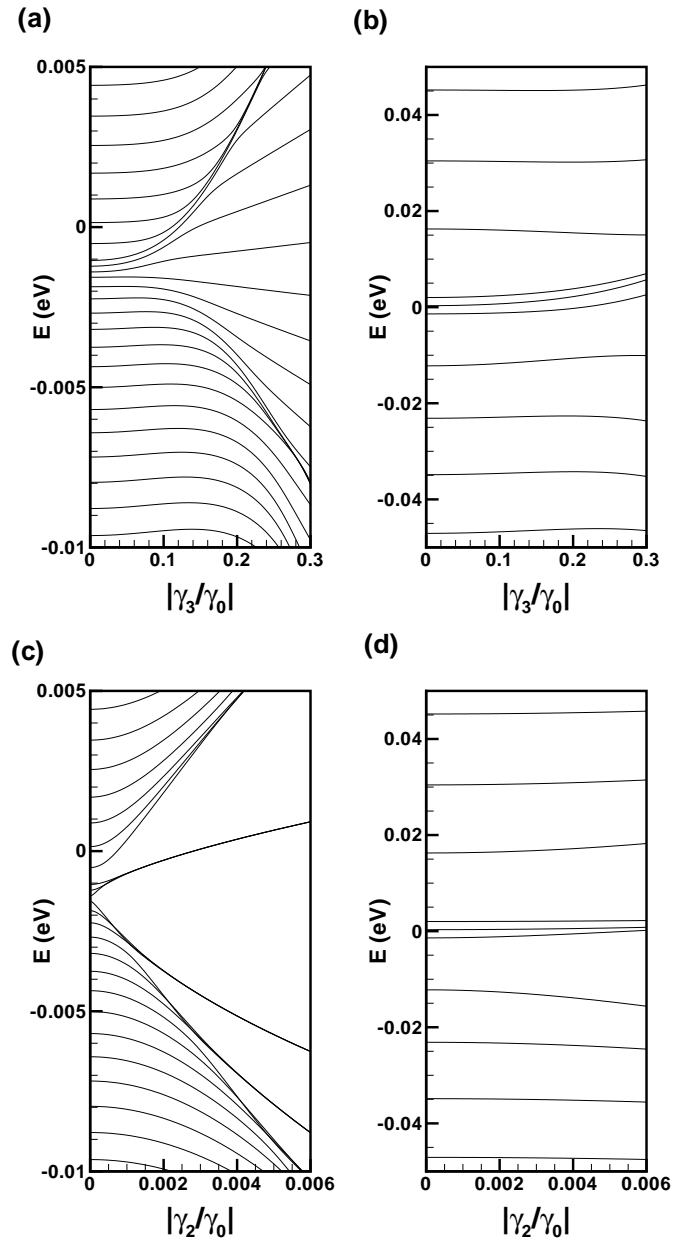


FIG. 4: Landau level spectrum in TLG at zero bias in the six-band model as a function of the ratio $|\gamma_3/\gamma_0|$ with $\gamma_2 = 0$ for (a) $B = 1$ T and (b) $B = 10$ T and as a function of the ratio $|\gamma_2/\gamma_0|$ with $\gamma_3 = 0$ for (c) $B = 1$ T and (d) $B = 10$ T.

Figure 4 (c),(d) shows the same analysis but with $\gamma_3 = 0$ and varying $|\gamma_2/\gamma_0|$. Again, the spectrum is strongly influenced by γ_2 at low field. It becomes independent of γ_2 at a magnetic field of the order of $B = 20$ T for our choice of hopping parameters i.e. $|\gamma_2/\gamma_0| = 0.0054$. This value is again in agreement with the analytical result given above. For TLG, it is necessary to go to much larger magnetic fields than in BLG to avoid the Landau level degeneracy caused by γ_2 and γ_3 .

C. Dispersion with magnetic field

In this section, we compute the dispersion of the first few Landau levels with magnetic field at zero bias. The result is shown in Fig. 5(a),(b) for BLG and Fig. 5(c),(d) for TLG. The black lines are for the full (4BM or 6BM) Hamiltonian while the blue squares are the 2BM dispersions. Figure 5 (b) and (d) shows an enlarged portion of the low-energy sector that contains the sub-levels in $M = 0$ i.e. $n = 0, 1$ for BLG and $n = 0, 1, 2$ for TLG.

For BLG, warping term γ_3 in the 4BM leads to a very small upward shift $\sim 10^{-4}$ eV of the $n = 0$ level with respect to the 2BM where this level is exactly at zero energy. (This small shift is also visible in Fig. 3 (b).) Otherwise, the 2BM overestimates the Landau level energies at all magnetic fields. The energy difference increases with magnetic field and with Landau level index. For example, at $B = 30$ T, the difference in energy between the 4BM and 2BM is 25%, 35% and 51% for $n = 1, M = 1$ and $M = 2$ respectively. For $n = 1$, the linear dependence of the energy predicted by the 2BM is lost at $B \approx 10$ T in the 4BM. For the higher Landau levels, the accuracy of the 2BM is poor excepted at small magnetic fields.

For TLG, the effects of γ_2, γ_3 are important for $B \lesssim 20$ T and, in this range of magnetic field, there is a great disparity between the full and 2BM even for the $n = 0, 1, 2$ levels in $M = 0$ whose energy is otherwise well estimated by the 2BM at higher magnetic field. The linear dependence of the energy with magnetic field given by the 2BM for $n = 0, 1, 2$ is only present for $B \gtrsim 10$ T in TLG. The energy difference between the 6BM and 2BM at $B = 30$ T is 0.1%, 16%, 18%, 39% and 59% for $n = 0, 1, 2$ and $M = 1, 2$ respectively. As in BLG, the energy difference between the full and 2BM increases with Landau level index $|M|$ and with magnetic field.

We showed above that, in BLG and TLG, the 2BM is expected to be valid for magnetic fields $B < 56$ T. In the numerical analysis, important quantitative differences between the 4BM and 2BM appear at magnetic fields much smaller than this value. In fact, the energy of the Landau level $M = 1$ at $B = 30$ T is already near the expected limit of validity of the 2BM which is $E \approx \gamma_1/4$.

For magnetic fields $B > 1$ T, the Landau level energies in our calculation converge for $N_{\max} = 100$. When the magnetic field is decreased, N_{\max} must be increased, however. In Fig. 5, we have set $N_{\max} = 900$. The \sqrt{B}

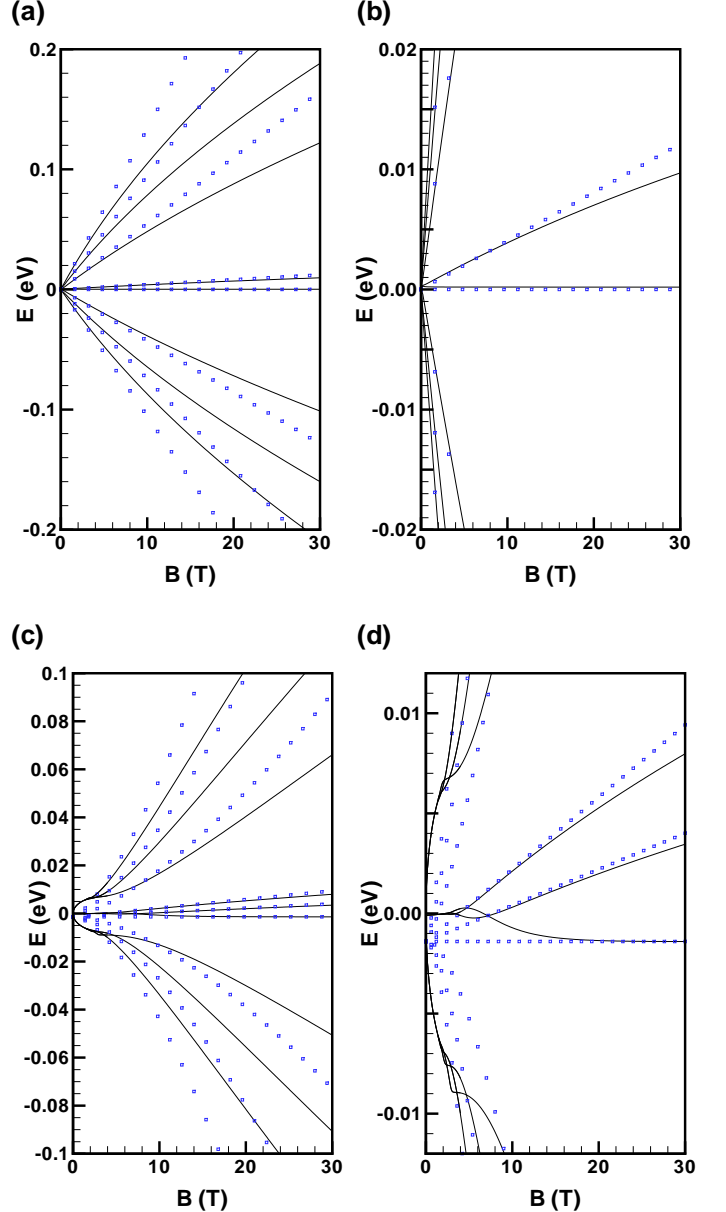


FIG. 5: (Color online) Behavior of the Landau levels with magnetic field at zero bias for valley K_+ for the four-band model (lines) and two-band model without γ_2 and γ_3 (blue squares). (a) bilayer graphene; (b) low-energy sector showing the $M = 0$ levels of (a); (c) trilayer graphene; (d) low-energy sector showing the $M = 0$ levels of (c).

behavior of the Landau level at small magnetic field in TLG is clearly visible in Fig. 5(c) and (d). As expected, the levels with small energy converge more rapidly with N_{\max} than those with high energy.

D. Dispersion with bias Δ_B

Figure 6 shows the dependence of the first Landau levels with bias for BLG for the 4BM (black lines) and the 2BM (blue squares) at magnetic fields $B = 10$ T and $B = 30$ T. The comparison between the two models is quite good in BLG for $M = 0$ (and even for $M = \pm 1$ at $B = 10$ T). For $|M| > 1$, however, the 2BM is quantitatively wrong and does not even give the correct qualitative dispersion with bias. This is not surprising since the Landau level energy for $|M| = 2$ is above $\gamma_1/4$.

To estimate the range of validity of the 2BM for the $M = 0$ levels, we consider the range of bias where the energies in the two models are close and where the $M = 0$ levels have lower energy than the $M = \pm 1$ levels. For $B = 10$ T and BLG, this range is roughly given by $\Delta_B \in [-0.1, 0.1]$ eV while for $B = 30$ T, it is extended to $\Delta_B \in [-0.22, 0.18]$. Note that a bias $\Delta_B = 0.1$ eV corresponds to an electric field of $E = 150$ mV/nm which is in the experimentally accessible range.²²

Because $\gamma_4 \neq 0$ in our calculation, the two levels in $M = 0$ in BLG meet at a finite negative (positive) bias Δ_B^* in valley $K_+(K_-)$ instead of at $\Delta_B^* = 0$. For $\Delta_B < \Delta_B^*$ (valley K_+) in Fig. 6, the order of the $n = 0, 1$ levels is reversed i.e. $E_{n=1} < E_{n=0}$. From Eqs. (14,15), $\Delta_B^* = -\delta_0 - 2\gamma_1\gamma_4/\gamma_0 = -0.046$ eV for the values of the hopping parameters considered in this paper. This change in the relative position of the $n = 0, 1$ energy levels leads to interesting physics when Coulomb interaction is introduced because the Coulomb exchange energy is more negative in level $n = 0$ than in level $n = 1$. The kinetic energy can thus compete with the exchange energy to create broken-symmetry states with orbital coherence when $E_{n=1} \leq E_{n=0}$.⁸ This state is characterized by a finite density of electric dipoles all pointing in the same direction in space.²³

Figure 7 shows the dependence of the first Landau levels with bias in TLG for the 6BM (black lines) and the 2BM (blue squares) at magnetic fields $B = 10$ T and $B = 30$ T. The γ_2 and γ_3 terms are important at $B = 10$ T and the range of validity of the 2BM for the $M = 0$ Landau levels is dramatically reduced to $\Delta_B \in [-0.032, 0.005]$ eV for $B = 10$ T. For $B = 30$ T, this range is extended to $\Delta_B \in [-0.14, 0.10]$ eV. In TLG, as in BLG, the range of validity increases with magnetic field. In TLG, however, there is a region around the crossing point of the $n = 0, 1, 2$ levels predicted in valley K_+ by the 2BM i.e. $\Delta_B^* = 2(\delta_0 + 2\gamma_1\gamma_4/\gamma_0) = -0.06$ eV, (i.e. in the range $\Delta_B \approx [-0.07, -0.05]$) where the 6BM gives three crossings of the $n = 0, 1, 2$ levels (see Fig. 8). The energy ordering of the levels with increasing bias is $n = (2, 1, 0) \rightarrow (2, 0, 1) \rightarrow (0, 2, 1) \rightarrow (0, 1, 2)$. The multiple crossings disappear if γ_4 is set to zero in which case there is a single crossing at the value predicted by the 2BM. This multiple crossing behavior is not captured by the 2BM. When Coulomb interaction is added to the picture, these multiple crossings should lead to a variety of broken-symmetry states with orbital coherence and so

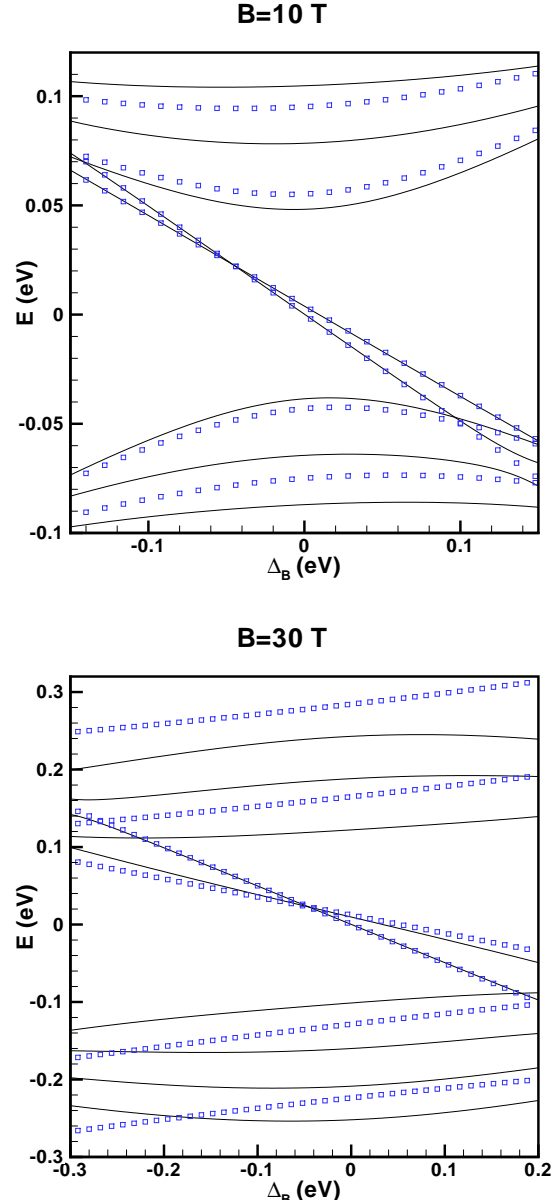


FIG. 6: (Color online) Dispersion of the first few Landau levels with bias for the four-band model (lines) and two-band model without γ_3 (blue squares) at magnetic field $B = 10$ T and $B = 30$ T for bilayer graphene.

to a rich phase diagram for the C2DEG in this range of bias.

E. Effect of the hopping terms on the Landau level spectrum

It is interesting to see the change in the Landau level spectrum as the different hopping terms are successively turned on at zero bias in TLG. This is shown in Fig. 9.

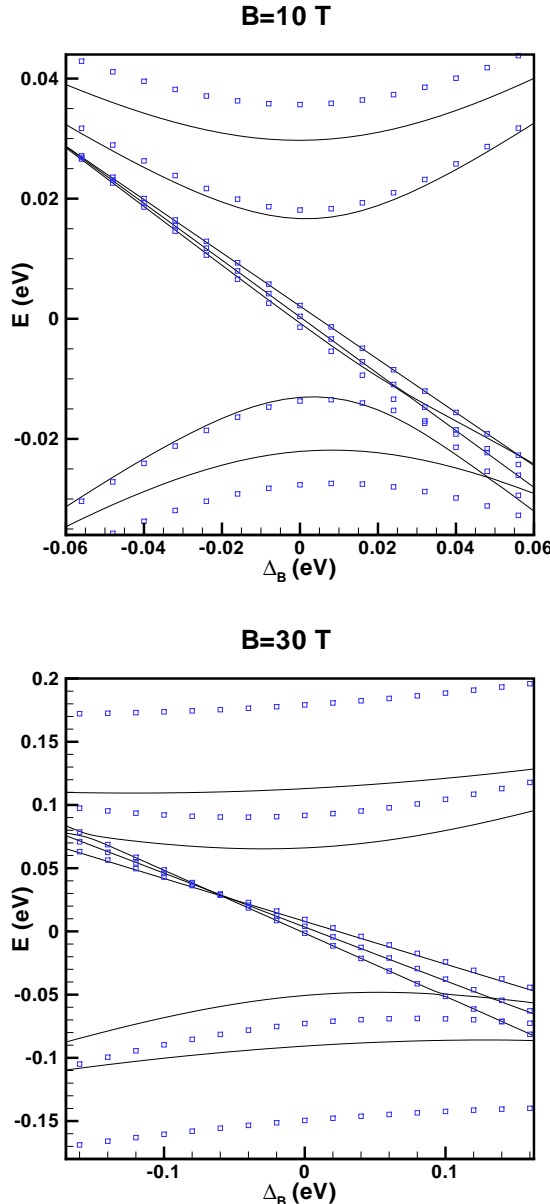


FIG. 7: (Color online) Dispersion of the first few Landau levels with bias for the six-band model (lines) and two-band model without γ_2, γ_3 (blue squares) at magnetic field $B = 10$ T and $B = 30$ T for trilayer graphene.

At the top of each figure, we indicate what hopping terms are non zero. In the minimal model with $\gamma_0, \gamma_1 \neq 0$ only showing that levels $n = 0, 1, 2$ in $M = 0$ are degenerate. With $\delta_0 \neq 0$ the spectrum is very slightly shifted downwards since $\delta_0 < 0$ and the degeneracy of the $n = 0, 1, 2$ levels is lifted. The energy of levels $n = 1, 2$ now depends linearly on the magnetic field (see Eqs. (24-26)). With $\gamma_4 \neq 0$ the downward shift is maintained and the slope of the $n = 0, 1, 2$ levels with magnetic field is increased. With the addition of γ_2 , the spectrum is shifted

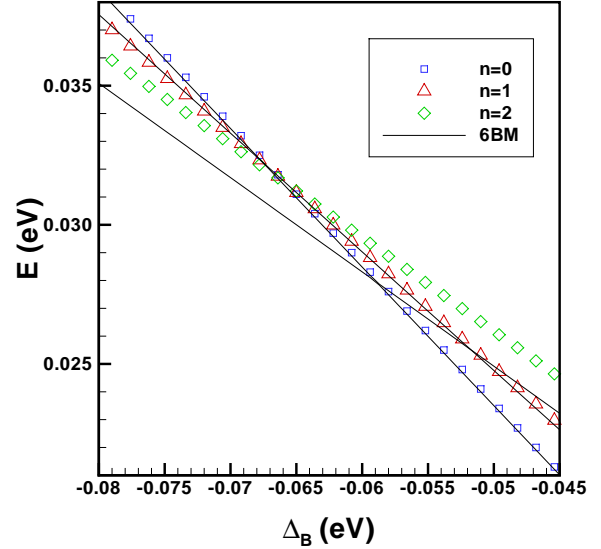


FIG. 8: (Color online) Dispersion of the three Landau levels $n = 0, 1, 2$ in $M = 0$ with bias in trilayer graphene at $B = 30$ T showing the multiple crossings in the 6BM (black lines). The symbols are for the 2BM without γ_2, γ_3 .

upwards and crossings occur between the $n = 0, 1, 2$ levels at small magnetic field (not visible in this figure but noticeable in Fig. 5 (d)). The dispersion of the higher energy levels with magnetic field changes from a \sqrt{B} behavior at small B to a $B^{3/2}$ behavior at larger magnetic field. This occurs at energies $\delta_0 - \gamma_2/2 = 0.007$ eV and $\delta_0 + \gamma_2/2 = -0.01$ eV. Groups of three levels become degenerate at very small magnetic field. (See also Refs. 11,24 where a similar band spectrum is presented.) Finally, the addition of γ_3 (see Fig. 5 (d)) leads to a small downward shift of the spectrum in Fig. 9 (d) but does not introduce other significant qualitative changes.

F. Eigenstates in the two- and six-band model

In BLG, the eigenspinors given by Eqs. (3) are coupled together by the hopping term γ_3 . In order to diagonalize the full Hamiltonian H_ξ , we used in Sec. II the basis $\{\Psi_{N=0,1}^{(0)}, \Psi_{N=1,1}^{(0)}, \Psi_{N=1,2}^{(0)}, \Psi_{N=1,3}^{(0)}, \Psi_{N>1,k}^{(0)}, \dots\}$ (with $k = 1, \dots, 4$) of the eigenstates of $H_\xi^{(0)}$ where the spinors $\Psi_{N,k}^{(0)}$ for a given N are ordered in ascending order of their energy $E_{N,k}^{(0)}$. The eigenstates $\Phi^{(j)}$ of H_ξ can be written as linear combinations of the basis spinors i.e.

$$\Phi^{(j)} = \sum_{J(N,k)} b_{J(N,k)}^{(j)} \Psi_{N,k}^{(0)}, \quad (29)$$

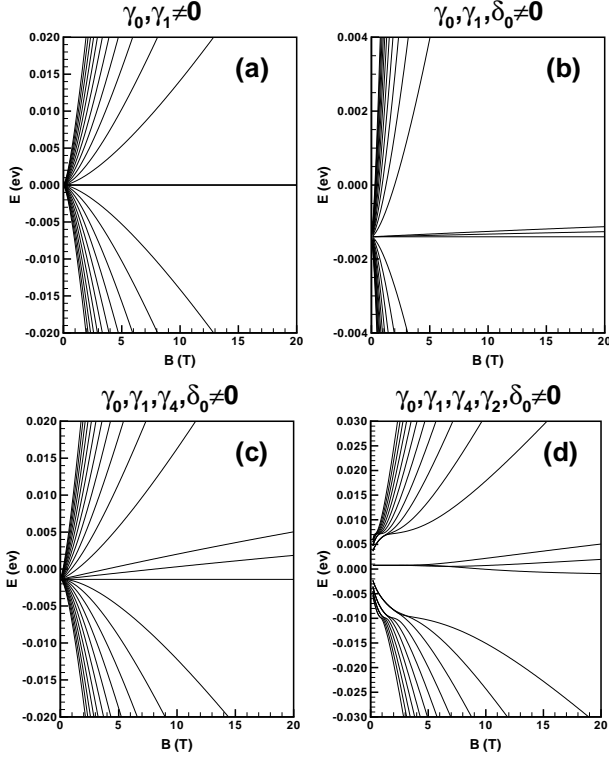


FIG. 9: Dispersion of the Landau levels with magnetic field at zero bias in the six-band model of trilayer graphene: (a) minimal model; (b) with the addition of δ_0 ; (c) with the further addition of δ_0 and γ_4 and (d) with the further addition of δ_0, γ_4 and γ_2 .

where the coefficients $b_k^{(j)}$ are obtained by numerically diagonalizing the full matrix H_ξ . If n_{vec} eigenspinors are kept, then $j, J = 1, \dots, n_{vec}$ with the super-index $J(N, k)$ defined by

$$J(0, 1) = 1, \quad (30)$$

$$J(1, 1) = 2, \quad (31)$$

$$J(1, 2) = 3, \quad (32)$$

$$J(1, 3) = 4, \quad (33)$$

$$J(N > 1, k) = 4(N - 1) + k. \quad (34)$$

In this section, we are interested in comparing the eigenstates of Landau level $M = 0$ in the 4BM or 6BM and 2BM. We start by considering BLG and later generalize the approach to TLG.

For BLG, the two eigenstates are the $n = 0, 1$ states that disperse linearly with bias in Fig. 6. In the 4BM, we denote these eigenstates by $\Phi^{(j_0)}$ and $\Phi^{(j_1)}$. In the absence of coupling due to the warping term,

$$\Phi^{(j_0)} = \Psi_{N=0,1}^{(0)} \implies b_1^{(j_0)} = 1, \quad (35)$$

$$\Phi^{(j_1)} = \Psi_{N=1,2}^{(0)} \implies b_3^{(j_1)} = 1, \quad (36)$$

and so the importance of the coupling can be measured

by computing the probabilities

$$P_0 = |b_1^{(j_0)}|^2, \quad (37)$$

$$P_1 = |b_3^{(j_1)}|^2. \quad (38)$$

The smaller the value of P_0, P_1 , the more important is the coupling.

In the 2BM, an electron in the j_0 or j_1 Landau level is assumed to reside mostly on site A_2 (for valley K_+) and to be described by the wave function $h_{0,X}(\mathbf{r})$ for j_0 and $h_{1,X}(\mathbf{r})$ for j_1 . According to Eq. (A14) in Appendix A, the occupation of the other sites are of order 2 in the small quantities defined in this Appendix. In the 4BM, however, the eigenstate is given by the spinor of Eq. (3) and for level j_1 , there may be some electronic amplitude on two other sites of the unit cell i.e. B_2 and A_1 . To measure how well the 2BM describes the 4BM eigenstate in levels j_0, j_1 , we define the probabilities

$$\Lambda_0 = P_0 |c_{N=0,1,2}|^2, \quad (39)$$

$$\Lambda_1 = P_1 |c_{N=1,3,2}|^2. \quad (40)$$

(Note that $|c_{N=0,1,2}|^2 = 1$ so that $P_0 = \Lambda_0$.)

We repeat the above procedure for the TLG system, defining in a similar way the probabilities P_n and Λ_n for $n = 0, 1, 2$. Our numerical results are shown in Fig. 10 for BLG and Fig. 11 for TLG.

Figure 10 shows the probabilities P_n and Λ_n as well as the dispersion of the $n = 0, 1$ levels with bias in BLG at magnetic field of (a) 10 T and (b) 30 T. The range of bias is $\Delta_B \in [-0.1, 0.1]$ eV for $B = 10$ T and $\Delta_B \in [-0.22, 0.18]$ eV for $B = 30$ T corresponding to the domain of validity for the 2BM established in Sec. III (C). In this figure, $P_0, P_1 \gtrsim 0.98$ at both magnetic fields and the warping term has very little effect on the eigenstate. The eigenvectors $\Psi_{N=0,1}^{(0)}$ and $\Psi_{N=1,2}^{(0)}$ are only slightly coupled to the other eigenstates of $H_\xi^{(0)}$. The coupling decreases with increasing magnetic field as noted before. The probability $\Lambda_0 \approx 0.98$ for $B = 10$ T and $\Lambda_0 \approx 0.99$ for $B = 30$ T so that the $n = 0$ 2BM eigenvector is a good approximation of the 4BM eigenvector in this case. For $n = 1, \Lambda_1 \approx 0.90$ for $B = 10$ T and $\Lambda_1 \approx 0.78$ for $B = 30$ T so that the 2BM eigenvector for $n = 1$ is not as good an approximation as the 2BM eigenvector for $n = 0$.

Figure 11 shows the probabilities P_n and Λ_n as well as the dispersion of the $n = 0, 1, 2$ levels with bias in TLG at magnetic field of (a) 10 T and (b) 30 T. The domain of validity of the 2BM is $\Delta_B \in [-0.032, 0.005]$ eV for $B = 10$ T and $\Delta_B \in [-0.14, 0.10]$ eV for $B = 30$. In this figure, $P_0, P_1, P_2 \gtrsim 0.96$ at $B = 30$ T and so both magnetic fields and the warping term has very little effect in this case. At the lower $B = 10$ T field, however, the coupling is noticeable for level $n = 0$. This is what causes the $n = 0$ Landau level to increase in energy for $B \lesssim 10$ T in Fig. 5 (d). As in BLG, the probabilities

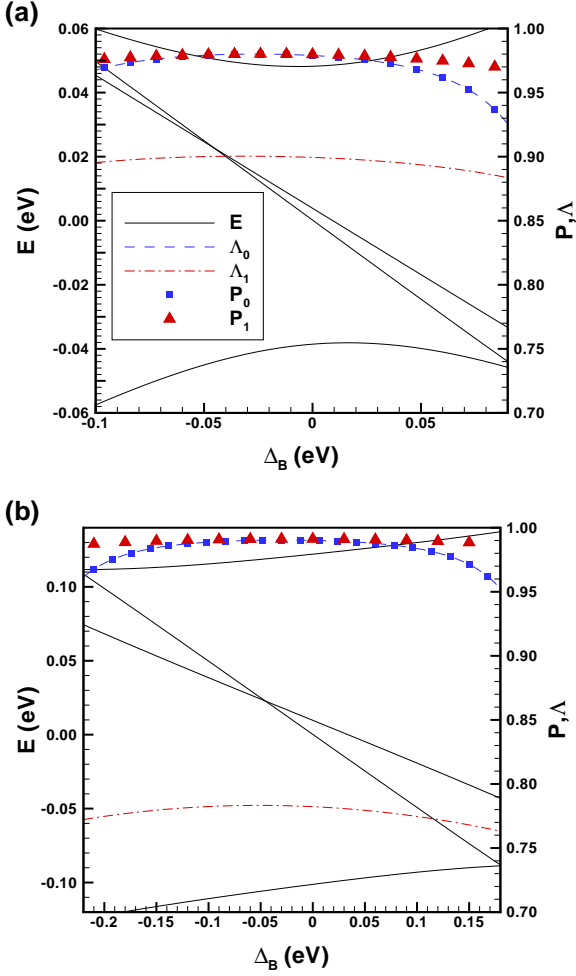


FIG. 10: (Color online) Low-energy eigenstates of the four-band model and the probabilities P and Λ as a function of bias for the $M = 0; n = 0, 1$ levels of bilayer graphene at (a) $B = 10$ T and (b) $B = 30$ T.

Λ_n decrease with magnetic field and so the amplitude of the wave function on sites other than those prescribed by the 2BM are not negligible for $B = 30$ T and $n = 1, 2$. In the region of the multiple crossings (in the range $\Delta_B \in [-0.07, -0.05]$), the levels $n = 0, 1, 2$ cross each other but do not become coupled. In consequence, each level keeps its orbital character in the sense that the amplitude of the wave function for level n is maximal in the orbital $h_n(\mathbf{r})$.

The fact that the electronic amplitude is not small on the high-energy sites at large magnetic field means that the physical quantities such as electric current and electromagnetic absorption are not correctly estimated in the 2BM.

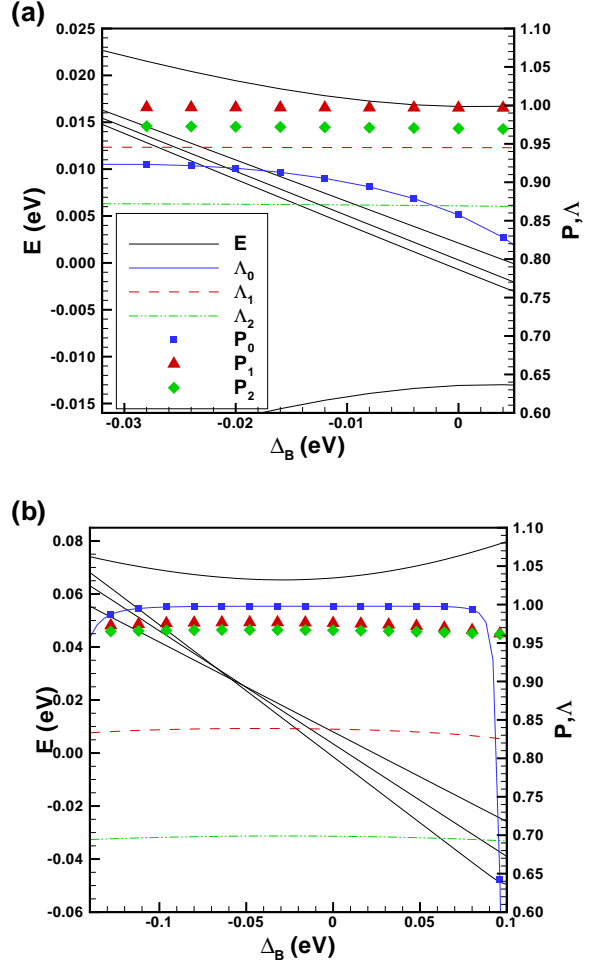


FIG. 11: (Color online) Low-energy eigenstates of the six-band model and the probabilities P and Λ as a function of bias for the $M = 0; n = 0, 1, 2$ levels of trilayer graphene at (a) $B = 10$ T and (b) $B = 30$ T.

IV. CONCLUSION

The two-band model is a useful approximation to study the transport and optical properties of the chiral two-dimensional electron gas in bilayer and trilayer graphene but it is important to know its range of applicability. In this paper, we have compared the Landau level spectrum of the full 6BM (TLG) and 4BM (BLG) as a function of magnetic field and bias with the predictions of the 2BM. We can summarize our main conclusions as follows: (a) the 2BM is generally a better approximation in BLG than in TLG; (b) it describes satisfactorily the $M = 0$ Landau levels but differences with the 4BM or 6BM spectrum increase rapidly with increasing Landau level index $|M|$ and magnetic field; (c) the coupling terms γ_3 in BLG and γ_2, γ_3 in TLG have little effect on the Landau level spectrum at magnetic field $B \gtrsim 1$ T in BLG and $B \gtrsim 10$ T in TLG; (d) at fixed magnetic field and varying bias,

the range of validity of the 2BM increases with magnetic field but is much smaller in TLG than in BLG; (e) for TLG, the multiple crossings between the $M = 0$ levels that occur within a small range of bias in the 6BM are not captured by the 2BM and so the 2BM may miss some interesting ground states of the C2DEG when Coulomb interaction is added to the non-interacting Hamiltonian; (f) the amplitude of the electronic wave function on sites other than those prescribed by the 2BM for the $M = 0$ eigenstates increases with magnetic field and is not negligible at large field; (g) the 2BM consistently overestimates the Landau level energies.

Acknowledgments

R. Côté was supported by a grant from the Natural Sciences and Engineering Research Council of Canada (NSERC). Computer time was provided by Calcul Québec and Compute Canada.

Appendix A: DERIVATION OF THE TWO-BAND MODEL

Combining the approaches found in Refs. 7,12, we introduce the two-band model in the following way. The eigenvalue equation to be solved can be written in the form

$$\begin{pmatrix} H_{1,1} & H_{1,2} \\ H_{2,1} & H_{2,2} \end{pmatrix} \begin{pmatrix} |\Psi_1\rangle \\ |\Psi_2\rangle \end{pmatrix} = \varepsilon \begin{pmatrix} |\Psi_1\rangle \\ |\Psi_2\rangle \end{pmatrix}, \quad (\text{A1})$$

with the normalization condition

$$\langle \Psi_1 | \Psi_1 \rangle + \langle \Psi_2 | \Psi_2 \rangle = 1, \quad (\text{A2})$$

where $H_{1,1}$ is the Hamiltonian for the low-energy sector, $H_{2,2}$ the Hamiltonian of the high-energy sector and $H_{1,2}, H_{2,1}$ the coupling terms. In BLG, $H_{i,j}$ are 2×2 matrices and Ψ_1, Ψ_2 have 2 elements. In TLG, $H_{1,1}$ is a 2×2 matrix, $H_{2,2}$ a 4×4 matrix and $H_{1,2}, H_{2,1}$ are 2×4 and 4×2 matrices respectively and Ψ_1 has 2 elements and Ψ_2 has 4. We want to derive an equation for the low-energy part Ψ_1 of the eigenspinor.

The eigenvalue equation is rewritten as

$$(H_{11} - \varepsilon I) |\Psi_1\rangle + H_{12} |\Psi_2\rangle = 0, \quad (\text{A3})$$

$$H_{21} |\Psi_1\rangle + (H_{22} - \varepsilon I) |\Psi_2\rangle = 0. \quad (\text{A4})$$

where I is the unit matrix. Solving for $|\Psi_2\rangle$ gives

$$|\Psi_2\rangle = -(H_{22} - \varepsilon I)^{-1} H_{21} |\Psi_1\rangle \quad (\text{A5})$$

so that

$$[(H_{11} - \varepsilon I) - H_{12} (H_{22} - \varepsilon I)^{-1} H_{21}] |\Psi_1\rangle = 0. \quad (\text{A6})$$

This is an exact equation.

Now, H_{22} can be diagonalized by the transformation

$$H_{22} = U D_{22} U^{-1} \quad (\text{A7})$$

where D_{22} is the diagonal matrix containing the eigenvalues of H_{22} . It follows that

$$\begin{aligned} (H_{22} - \varepsilon I)^{-1} &= (U (D_{22} - \varepsilon I) U^{-1})^{-1} \\ &= U (D_{22} - \varepsilon I)^{-1} U^{-1}. \end{aligned} \quad (\text{A8})$$

For the low energy excitations, all eigenvalues of $D_{22} \gg \varepsilon$ so that

$$\frac{1}{d_{22} - \varepsilon} \approx \frac{1}{d_{22}} \left(1 + \frac{\varepsilon}{d_{22}} \right). \quad (\text{A9})$$

Hence,

$$(D_{22} - \varepsilon I)^{-1} \approx D_{22}^{-1} (I + \varepsilon D_{22}^{-1}), \quad (\text{A10})$$

and so

$$(H_{22} - \varepsilon I)^{-1} \approx H_{22}^{-1} (I + \varepsilon H_{22}^{-1}) \quad (\text{A11})$$

to first order in ε .

The Schrödinger equation now becomes

$$H_{eff} |\Psi_1\rangle = \varepsilon |\Psi_1\rangle, \quad (\text{A12})$$

where

$$H_{eff} = (I + H_{12} H_{22}^{-2} H_{21})^{-1} (H_{11} - H_{12} H_{22}^{-1} H_{21}). \quad (\text{A13})$$

We have also,

$$\begin{aligned} |\Psi_2\rangle &= -(H_{22} - \varepsilon I)^{-1} H_{21} |\Psi_1\rangle \\ &\approx -H_{22}^{-1} (I + \varepsilon H_{22}^{-1}) H_{21} |\Psi_1\rangle. \end{aligned} \quad (\text{A14})$$

In order to satisfy the normalization condition of the original model, we define

$$S = I + H_{12} H_{22}^{-2} H_{21} \quad (\text{A15})$$

and make the transformation

$$|\tilde{\Psi}_1\rangle = S^{1/2} |\Psi_1\rangle. \quad (\text{A16})$$

The new eigenvalue equation is

$$\tilde{H}_{eff} |\tilde{\Psi}_1\rangle = \varepsilon |\tilde{\Psi}_1\rangle \quad (\text{A17})$$

with

$$\begin{aligned} \tilde{H}_{eff} &= S^{1/2} H_{eff} S^{-1/2} \\ &= S^{-1/2} (H_{11} - H_{12} H_{22}^{-1} H_{21}) S^{-1/2}. \end{aligned} \quad (\text{A18})$$

Note that using Eq. (A14), we can further approximate

$$|\Psi_2\rangle \approx -H_{22}^{-1} H_{21} |\Psi_1\rangle, \quad (\text{A19})$$

so that it is easy to show that

$$\langle \tilde{\Psi}_1 | \tilde{\Psi}_1 \rangle \approx \langle \Psi_1 | \Psi_1 \rangle + \langle \Psi_2 | \Psi_2 \rangle = 1. \quad (\text{A20})$$

The Hamiltonians H_{eff} and \tilde{H}_{eff} have the same eigenvalues but \tilde{H}_{eff} is Hermitian while H_{eff} is not necessarily Hermitian.

The intralayer hopping γ_0, γ_1 are much larger than the small quantities $|\varepsilon|, |\gamma_2|, |\gamma_3|, |\gamma_4|, |\delta_0|, |\Delta_B|$. Keeping

only the terms that are linear in the small quantities and quadratic (BLG) or cubic (TLG) in the operators a, a^\dagger leads to the Hamiltonian for BLG and TLG given in the text. Within this approximation, \tilde{H}_{eff} and H_{eff} are identical and the normalization condition reduces to $\langle \Psi_1 | \Psi_1 \rangle = 1$ meaning that there is no amplitude of the wave function on the high-energy sites. (From Eq. (A14), the probability to be on a high-energy site is quadratic in the small quantities.)

¹ Edward McCann and Vladimir I. Fal'ko, Phys. Rev. Lett. **96**, 086805 (2006).

² For a review of the C2DEG, see: Yafis Barlas, Kun Yang, and A. H. MacDonald, Nanotechnology **23**, 052001 (2012).

³ Hongki Min and A. H. MacDonald, Phys. Rev. B **77**, 155416 (2008).

⁴ A. H. Castro Neto, F. Guinea, N. M. R. Peres, K. S. Novoselov and A. K. Geim, Rev. Mod. Phys. **81**, 109 (2009).

⁵ D. S. L. Abergel, V. Apalkov, J. Berashevich, K. Ziegler and Tapash Chakraborty, Advances in Physics **59**, 261 (2010).

⁶ M. O. Goerbig, Rev. Mod. Phys. **83**, 1193 (2011).

⁷ Edward McCann and Mikito Koshino, Rep. Prog. Phys. **76**, 056503 (2013).

⁸ J. Lambert and R. Côté, Phys. Rev. B **87**, 115415 (2013).

⁹ Yafis Barlas, R. Côté, and Maxime Rondeau, Phys. Rev. Lett. **109**, 126804 (2012).

¹⁰ R. Côté, Maxime Rondeau, Anne-Marie Gagnon, and Yafis Barlas, Phys. Rev. B **86**, 125422 (2012).

¹¹ Mikito Koshino and Edward McCann, Phys. Rev. B **80**, 165409 (2009).

¹² Fan Zhang, Bhagawan Sahu, Hongki Min, and A. H. MacDonald, Phys. Rev. B **82**, 035409 (2010).

¹³ See for example: Rahul Nandkishore and Leonid Levitov, Phys. Scr. T **146**, 015011 (2012); E. V. Gorbar, V. P. Gusynin, and V. A. Miransky, Phys. Rev. B **81**, 155451 (2010); JETP Lett. **91**, 314 (2010) [Pis'ma v ZhETF **91**, 334 (2010)]; E. V. Gorbar, V. P. Gusynin, V. A. Miransky, and I. A. Shovkovy, Phys. Rev. B **85**, 235460 (2012); E. V. Gorbar, V. P. Gusynin, Junji Jia, and V. A. Miransky, Phys. Rev. B **84**, 235449 (2011); E. V. Gorbar, V. P. Gusynin, A. B. Kuzmenko, and S. G. Sharapov, Phys. Rev. B **86**, 075414 (2012); K. Shizuya, Phys. Rev. B **79**, 165402 (2009); T. Misumi and K. Shizuya, Phys. Rev. B **77**, 195423 (2008).

¹⁴ Fan Zhang, Dagim Tilahun, and A. H. MacDonald, Phys. Rev. B **85**, 165139 (2012).

¹⁵ F. Guinea, A. H. Castro Neto, and N. M. R. Peres, Phys. Rev. B **73**, 245426 (2006).

¹⁶ Shengjun Yuan, Rafael Roldán, and Mikhail I. Katsnelson, Phys. Rev. B **84**, 125455 (2011).

¹⁷ J. Milton Pereira, Jr., F. M. Peeters, and P. Vasilopoulos, Phys. Rev. B **76**, 115419 (2007).

¹⁸ Eduardo V Castro, K. S. Novoselov, S. V. Morozov, N. M. R. Peres, J. M. B. Lopes dos Santos, Johan Nilsson, F. Guinea, A. K. Geim and A. H. Castro Neto, J. Phys.: Condens. Matter **22**, 175503 (2010).

¹⁹ B. Partoens and F. M. Peeters, Phys. Rev. B **74**, 075404 (2006).

²⁰ Johan Nilsson, A. H. Castro Neto, F. Guinea, and N. M. R. Peres, Phys. Rev. B **78**, 045405 (2008).

²¹ A. Grüneis, C. Attaccalite, L. Wirtz, H. Shiozawa, R. Saito, T. Pichler, and A. Rubio, Phys. Rev. B **78**, 205425 (2008).

²² R. T. Weitz, M. T. Allen, B. E. Feldman, J. Martin, and A. Yacoby, Science **330**, 812 (2010); Seyoung Kim, Kayoung Lee, and E. Tutuc, Phys. Rev. Lett. **107**, 016803 (2011).

²³ K. Shizuya, Phys. Rev. B **79**, 165402 (2009).

²⁴ Takahiro Morimoto, Mikito Koshino, and Hideo Aoki, Phys. Rev. B **86**, 155426 (2012).